



<b>Title</b>	<b>Effect of annealing on the performance of CrO<sub>3</sub>/ZnO light emitting diodes</b>
<b>Author(s)</b>	<b>Xi, YY; Ng, AMC; Hsu, YF; Djuriši, AB; Huang, BQ; Ge, L; Chen, XY; Chan, WK; Tam, HL; Cheah, KW</b>
<b>Citation</b>	<b>Applied Physics Letters, 2009, v. 94 n. 20</b>
<b>Issued Date</b>	<b>2009</b>
<b>URL</b>	<b><a href="http://hdl.handle.net/10722/58443">http://hdl.handle.net/10722/58443</a></b>
<b>Rights</b>	<b>Applied Physics Letters. Copyright © American Institute of Physics.</b>

## Effect of annealing on the performance of CrO<sub>3</sub>/ZnO light emitting diodes

Y. Y. Xi,<sup>1</sup> A. M. C. Ng,<sup>1</sup> Y. F. Hsu,<sup>1</sup> A. B. Djurišić,<sup>1,a)</sup> B. Q. Huang,<sup>1</sup> L. Ge,<sup>1</sup> X. Y. Chen,<sup>1</sup> W. K. Chan,<sup>2</sup> H. L. Tam,<sup>3</sup> and K. W. Cheah<sup>3</sup>

<sup>1</sup>Department of Physics, The University of Hong Kong, Pokfulam Road, Hong Kong

<sup>2</sup>Department of Chemistry, The University of Hong Kong, Pokfulam Road, Hong Kong

<sup>3</sup>Department of Physics, Hong Kong Baptist University, Kowloon Tong, Hong Kong

(Received 2 September 2008; accepted 22 April 2009; published online 20 May 2009)

Heterojunction CrO<sub>3</sub>/ZnO light emitting diodes have been fabricated. Their performance was investigated for different annealing temperature for ZnO nanorods. Annealing in oxygen atmosphere had significant influence on carrier concentration in the nanorods, as well as on the emission spectra of the nanorods. Surprisingly, annealing conditions, which yield the lowest band edge-to-defect emission ratio in the photoluminescence spectra, result in the highest band edge-to-defect emission ratio in the electroluminescence spectra. The influence of the native defects on ZnO light emitting diode performance is discussed. © 2009 American Institute of Physics. [DOI: 10.1063/1.3140962]

ZnO is a wide band gap material of great interest for applications in optoelectronic devices, such as light emitting diodes (LEDs).<sup>1–7</sup> Both homojunction<sup>7</sup> and heterojunction<sup>1–6</sup> devices, for a variety of materials, such as NiO,<sup>1</sup> GaN,<sup>2</sup> Si,<sup>3,6</sup> SrCuO<sub>2</sub>,<sup>4</sup> Cu<sub>2</sub>O,<sup>5</sup> *p*-type polymer,<sup>6</sup> etc., have been achieved. Significant differences in electroluminescence (EL) spectra and threshold voltages have been achieved for these devices, and often the emission spectra had a significant component in the visible spectral range.<sup>1–3,5,6</sup> Thus, investigation of different *p*-type materials for ZnO heterojunction LEDs is of interest. One of desirable features of the *p*-type material for ZnO heterojunction LEDs is inexpensive fabrication to preserve one of the main advantages of the use of ZnO (low cost). In this work, we have fabricated ZnO heterojunction LEDs with electrodeposited chromium (VI) oxide (CrO<sub>3</sub>) as a *p*-type layer. The influence of annealing conditions on device performance has been investigated since annealing has significant effect on the optical<sup>8–10</sup> and electronic properties<sup>10–12</sup> of ZnO.

The electrodeposition of chromium (III) hydroxide film (converted to CrO<sub>3</sub> after annealing) was carried out using a simple two electrode system [an indium tin oxide (ITO) coated glass anode and a Pt wire cathode] at room temperature at 2.8 V voltage (deposition time 1 min). The electrolyte was a solution containing 0.04M chromium (III) nitrate nonahydrate (Aldrich, 99.99+%) and 0.015M hexamethylene tetramine (HMT) (Aldrich, 99+ % ACS reagent) in a mixture of deionized water and ethanol (volume ratio: 1:1). The electrodeposited chromium hydroxide layer was then annealed at 200 °C for 30 min to convert it to chromium oxide. ZnO seed layer for ZnO nanorod growth was also electrodeposited using a two electrode system but with Zn foil anode, aqueous solution containing 0.04M zinc nitrate hydrate (Aldrich, 99.999%) and 0.015M HMT as an electrolyte, and at deposition temperature 80 °C. The voltage during deposition was 0.8 V and the deposition time was 1 min. The nanorods were then fabricated by a hydrothermal method<sup>8,9,13,14</sup> in an aqueous solution containing polyethyleneimine (Aldrich, 50 wt % in water), 0.025M zinc nitrate hydrate and 0.025M HMT at 90 °C for 2.5 h. Annealing was performed in a tube furnace

under the flow of oxygen gas at temperatures 200, 400, or 600 °C.

The morphology of samples was studied by scanning electron microscopy (SEM) using JEOL (JSM-7001F) SEM, while the optical properties were examined by photoluminescence (PL) spectroscopy using a HeCd laser (325 nm) and a PDA-512\_USB (Control Development Inc.) fiberoptic spectrometer. The electronic properties were investigated by electrochemical impedance spectroscopy (EIS) measurements.<sup>15</sup> The EIS measurement was performed in a three-electrode cell using a Pt wire as counter electrode and a standard Ag/AgCl in 3M KCl as reference electrode. The electrolyte was a 0.5M Na<sub>2</sub>SO<sub>4</sub> aqueous solution. The measurement was done by applying a 10 mV amplitude as signal over the constant applied bias with the frequency ranging between 10 000 and 0.05 Hz. Carrier concentrations were calculated from EIS data according to the procedure described in Ref. 15. For CrO<sub>3</sub> layer, *p*-type conductivity was confirmed using a hot-point probe method.<sup>16</sup>

For the device fabrication, a spin-on-glass (SOG) (Futurex, Inc.) layer was used to prevent short circuit after deposition of the top contact, since an insulating layer is needed to cover the area between the nanorods.<sup>1,2,6</sup> SOG was spin coated on ZnO nanorods at 3000 rpm and annealed in air at 200 °C for 1 min, resulting in thickness of ~400–500 nm (for 600–700 nm long ZnO rods). It should be noted that the thickness and the quality of insulating SOG layer are strongly dependent on the solution viscosity, which increases with the storage time of SOG solution. The Al electrode (100 nm) was deposited using a thermal evaporator AST PEVA 500 EL. For the EL and *I*-*V* measurements, a Keithley 2400 source meter and a monochromator (Acton SpectraPro 500i) with Peltier-cooled photomultiplier detector (Hamamatsu R636–10) were used. Optical power was measured using a Newport 1830-C optical power meter equipped with a 818-UV detector probe.

Figure 1 shows the SEM images of CrO<sub>3</sub> film and ZnO nanorods grown on CrO<sub>3</sub> film, as well as x-ray diffraction (XRD) spectrum of electrodeposited film before and after annealing and schematic diagram of a device. The observed peaks in the XRD spectra before annealing correspond to Cr(OH)<sub>3</sub>,<sup>17</sup> while after annealing at 200 °C peaks from CrO<sub>3</sub> (Ref. 18) can be observed. In both cases, some of the peaks

<sup>a)</sup>Electronic mail: dalek@hkusua.hku.hk.

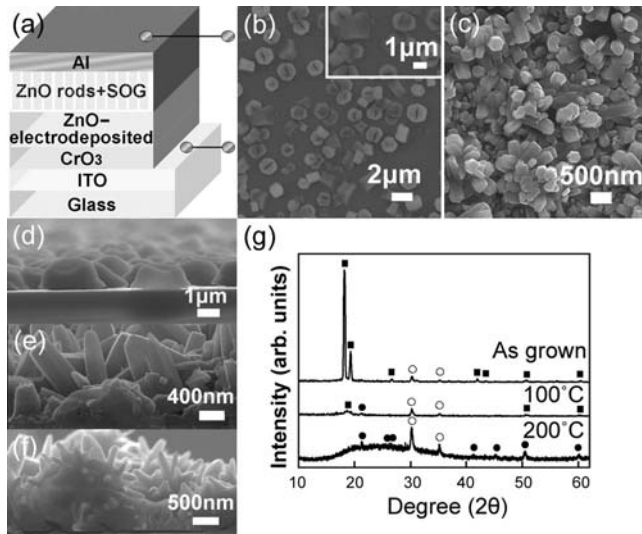


FIG. 1. (a) Schematic diagram of  $\text{CrO}_3/\text{ZnO}$  LED. Top-view SEM images of (b)  $\text{CrO}_3$  film and (c) ZnO nanorods on  $\text{CrO}_3$  film. Cross-sectional SEM images of (d)  $\text{CrO}_3$ , (e)  $\text{CrO}_3/\text{ZnO}$ , and (f)  $\text{CrO}_3/\text{ZnO}+\text{SOG}$ . (g) XRD spectra of  $\text{CrO}_3$  film (before and after annealing). Black squares, black circles and open circles denote peaks corresponding to  $\text{Cr}(\text{OH})_3$ ,  $\text{CrO}_3$ , and ITO, respectively.

corresponding to the ITO substrate<sup>19</sup> can also be found. It has been shown previously that presence of Cr (VI) is detected by x-ray absorption spectroscopy after annealing of chromium hydroxide at  $\sim 200^\circ\text{C}$ , and that full transformation to  $\text{Cr}_2\text{O}_3$  occurs at temperatures exceeding  $700^\circ\text{C}$ .<sup>20</sup> Annealing of the rods in oxygen atmosphere at temperature up to  $600^\circ\text{C}$  does not result in a change of morphology.

Figure 2 shows the PL spectra of the devices for different annealing temperatures. All the peaks originate from ZnO nanorods. As-grown ZnO nanorods exhibit a weak UV emission and a strong yellow-green defect emission commonly observed in hydrothermally grown samples.<sup>8,9</sup> Similar trends can be observed in ZnO nanorods fabricated here (electrodeposited seed) and those fabricated on ZnO nanoparticle seed or seed layer prepared from zinc acetate solutions.<sup>8,9</sup> In all cases, annealing at or above  $200^\circ\text{C}$  produces redshift of the defect emission. This can be attributed to the desorption of OH groups,<sup>8,9</sup> which are commonly present in hydrothermally grown samples and were found to be related to the presence of yellow-green emission.<sup>8,9,21</sup> The lowest UV to visible emission ratio is obtained for annealing at  $400^\circ\text{C}$ , in agreement with results obtained for ZnO nanorods grown on different seed layers.<sup>8,9</sup> The origin of various visible defect

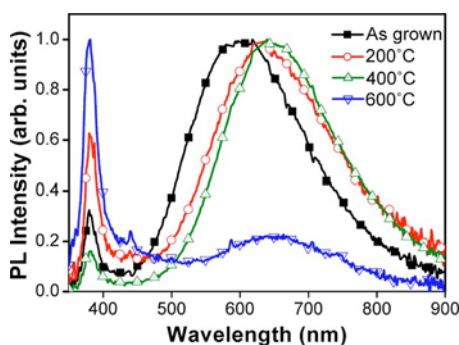


FIG. 2. (Color online) Normalized PL spectra of  $\text{CrO}_3/\text{ZnO}$  (annealed at different temperatures).

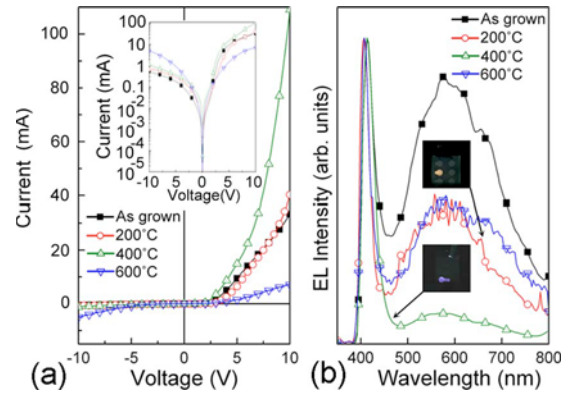


FIG. 3. (Color online) (a)  $I$ - $V$  curves (the inset shows logarithmic scale). (b) Normalized EL spectra (biased at 18–19 V) of different  $\text{CrO}_3/\text{ZnO}$  LEDs. The insets show corresponding photos to representative spectra.

emission peaks in ZnO is still debated.<sup>22</sup> The fact that the observed emission peak is reduced after annealing in oxygen at  $600^\circ\text{C}$  indicates that this emission is likely not due to defects associated with excess oxygen<sup>22</sup> but rather defect complexes instead of single point defects.<sup>9</sup>

Annealing in oxygen also results in decrease in the carrier concentration ( $\sim 3.5 \times 10^{21} \text{ cm}^{-3}$  for as-grown,  $\sim 6.5 \times 10^{19} \text{ cm}^{-3}$  for  $200^\circ\text{C}$ ,  $\sim 8.7 \times 10^{19} \text{ cm}^{-3}$  for  $400^\circ\text{C}$ , and  $\sim 1.4 \times 10^{19} \text{ cm}^{-3}$  for  $600^\circ\text{C}$ ) in agreement with obtained results for ZnO thin films.<sup>12</sup> The measured  $I$ - $V$  curves and EL spectra for different annealing conditions are shown in Fig. 3. The observed changes in the carrier concentration are due to the change in concentrations of native defects, though OH group desorption (occurring at  $\sim 150^\circ\text{C}$ )<sup>9,23</sup> could also play a role. The turn-on voltages for the light emission (8 V for as-grown, 9 V for  $200^\circ\text{C}$  annealing and 10 V for 400 and  $600^\circ\text{C}$ ) do not follow the same trends as the  $I$ - $V$  curves, where the highest currents for the same bias voltage are obtained for samples annealed at  $400^\circ\text{C}$ . Also, there is no obvious relationship between the measured  $I$ - $V$  curves and the carrier concentrations in ZnO nanorods, indicating additional factors, such as interface quality and energy level alignment at the interface, which affect the carrier injection and recombination. It has been shown that annealing<sup>24</sup> or deposition conditions<sup>25</sup> can alter the energy level alignment in ZnO-based heterojunctions, which can occur due to changes in the position of the surface Fermi level<sup>24</sup> or changes in the local composition of the interface<sup>25</sup> and interface dipoles.<sup>24,25</sup> Also, rectifying properties worsen in case of annealing at  $600^\circ\text{C}$ . Ideality factors for all devices are large. Previously reported heterojunctions between ZnO nanowires and  $p$ -Si also exhibited high ideality factors, which was attributed to the fact that this junction needed to be described as a series of diodes (and consequently ideality factor would be a sum of ideality factors of individual diodes) and deep-level-assisted tunneling.<sup>26</sup> Both of these mechanisms could contribute to the observed  $I$ - $V$  curve behavior in our study.

We can also observe a dramatic difference between the measured EL and PL spectra. The samples annealed at  $400^\circ\text{C}$  exhibit prominent defect emission peak in PL, and only a weak defect emission in EL. The reasons for observed differences between EL and PL spectra are the differences in excitation mechanism. In PL, electron-hole pairs are created in the region within optical penetration depth of the excitation source.<sup>27</sup> In EL, nonequilibrium carriers are injected at



electrodes and transported to the junction.<sup>27</sup> This process can result in carrier trapping in the bulk or the interface,<sup>27</sup> as well as carrier accumulation at interface in case of large injection barriers. Consequently, in presence of a variety of native defects as in the case of ZnO, there can be considerable differences between EL and PL spectra. In some cases, strong UV emission is obtained in PL and only weak visible defect emission is obtained in EL,<sup>27</sup> while here the opposite behavior is observed for samples annealed at 400 °C. These results indicate great impact of defects on properties and device performance of ZnO.

We have previously observed that strong short wavelength emission can be obtained at higher bias for NiO/ZnO devices which exhibited prominent defect emission in PL spectra. In these devices, the ratio between the UV and defect emission peak increased with increased bias voltage.<sup>1</sup> However, no significant changes in this ratio are observed in devices with chromium oxide *p*-type layer. On the other hand, there is considerable redshift of the emission peak (for example, from 398 nm at 12 V to 404 nm at 16 V for as-grown sample, and 404 nm at 12 V to 416 nm at 16 V for 600 °C sample), with the largest shift (from 392 nm at 12 V to 410 nm at 16 V) observed for the device with 400 °C annealing temperature. The emitted power from this device at 13 V bias is 0.32 μW/cm<sup>2</sup>. The redshift is likely due to the increase of the temperature of the active region, considering relatively large current density. Such effects have been previously observed in other types of devices and can be reduced either by optimizing device architecture and growth conditions to increase efficiency and decrease parasitic resistance or by pulsed excitation.<sup>28</sup>

To summarize, we have fabricated LEDs based on CrO<sub>3</sub>/ZnO heterojunctions and investigated the influence of the annealing on the optical and electronic properties. Large differences were obtained between EL and PL spectra of the devices, and both types of luminescence spectra as well as the *I*-*V* curves exhibited strong dependence on the annealing conditions. The observed phenomena were attributed to the changes in native defect concentrations after annealing.

Financial support from the Strategic Research Theme, University Development Fund, Seed Funding Grant, Outstanding Young Researcher Award (administrated by The University of Hong Kong), Hung Hing Ying Physical Sciences Research Fund, and Innovation & Technology Fund (Grant No. ITS/129/08) is acknowledged. The authors would

like to thank Professor K. Y. Chan for the use of equipment for EIS measurements.

- <sup>1</sup>Y. Y. Xi, Y. F. Hsu, A. B. Djurišić, A. M. C. Ng, W. K. Chan, H. L. Tam, and K. W. Cheah, *Appl. Phys. Lett.* **92**, 113505 (2008).
- <sup>2</sup>W. I. Park and G.-C. Yi, *Adv. Mater. (Weinheim, Ger.)* **16**, 87 (2004).
- <sup>3</sup>J. D. Ye, S. L. Gu, S. M. Zhu, W. Liu, S. M. Liu, R. Zhang, Y. Shi, and Y. D. Zheng, *Appl. Phys. Lett.* **88**, 182112 (2006).
- <sup>4</sup>H. Ohta, K. Kawamura, M. Orita, M. Hirano, N. Sarukura, and H. Hosono, *Appl. Phys. Lett.* **77**, 475 (2000).
- <sup>5</sup>I. T. Drapak, *Sov. Phys. Semicond.* **2**, 513 (1968).
- <sup>6</sup>C. S. Rout and C. N. R. Rao, *Nanotechnology* **19**, 285203 (2008).
- <sup>7</sup>Z. P. Wei, Y. M. Lu, D. Z. Shen, Z. Z. Zhang, B. Yao, B. H. Li, J. Y. Zhang, D. X. Zhao, X. W. Fan, and Z. K. Tang, *Appl. Phys. Lett.* **90**, 042113 (2007).
- <sup>8</sup>K. H. Tam, C. K. Cheung, Y. H. Leung, A. B. Djurišić, C. C. Ling, C. D. Beling, S. Fung, W. M. Kwok, W. K. Chan, D. L. Phillips, L. Ding, and W. K. Ge, *J. Phys. Chem. B* **110**, 20865 (2006).
- <sup>9</sup>A. B. Djurišić, Y. H. Leung, K. H. Tam, Y. F. Hsu, L. Ding, W. K. Ge, Y. C. Zhong, K. S. Wong, W. K. Chan, H. L. Tam, K. W. Cheah, W. M. Kwok, and D. L. Phillips, *Nanotechnology* **18**, 095702 (2007).
- <sup>10</sup>Y. F. Hsu, Y. Y. Xi, A. B. Djurišić, and W. K. Chan, *Appl. Phys. Lett.* **92**, 133507 (2008).
- <sup>11</sup>Q. Zhao, X. Y. Xu, X. F. Song, D. P. Yu, C. P. Li, and L. Guo, *Appl. Phys. Lett.* **88**, 033102 (2006).
- <sup>12</sup>H. S. Kang, J. S. Kang, J. W. Kim, and S. Y. Lee, *J. Appl. Phys.* **95**, 1246 (2004).
- <sup>13</sup>M. Law, L. E. Greene, J. C. Johnson, R. Saykally, and P. Yang, *Nature Mater.* **4**, 455 (2005).
- <sup>14</sup>L. E. Greene, M. Law, D. H. Tan, M. Montano, J. Goldberger, G. Somorjai, and P. Yang, *Nano Lett.* **5**, 1231 (2005).
- <sup>15</sup>I. Mora-Seró, F. Fabregat-Santiago, B. Denier, J. Bisquert, R. Tena-Zaera, J. Elias, and C. Levy-Clement, *Appl. Phys. Lett.* **89**, 203117 (2006).
- <sup>16</sup>G. Golan, A. Axelevitch, B. Gorenstein, and V. Manevych, *Microelectron. J.* **37**, 910 (2006).
- <sup>17</sup>JCPDS Card. No. 12-0241.
- <sup>18</sup>JCPDS Card. No. 77-0125.
- <sup>19</sup>JCPDS Card. No. 39-1058.
- <sup>20</sup>S. L. M. Schroeder, G. D. Moggridge, T. Rayment, and R. M. Lambert, *J. Phys. Chem.* **IV** **7**, 923 (1997).
- <sup>21</sup>N. S. Norberg and D. R. Gamelin, *J. Phys. Chem. B* **109**, 20810 (2005).
- <sup>22</sup>A. B. Djurišić and Y. H. Leung, *Small* **2**, 944 (2006).
- <sup>23</sup>R. G. Xie, D. S. Li, D. R. Yang, T. Sekiguchi, and M. H. Jiang, *Nanotechnology* **17**, 2789 (2006).
- <sup>24</sup>D. C. Olson, Y.-J. Lee, M. S. White, N. Kopidakis, S. E. Shaheen, D. S. Ginley, J. A. Voigt, and J. W. P. Hsu, *J. Phys. Chem. C* **112**, 9544 (2008).
- <sup>25</sup>H. F. Liu, G. X. Hu, H. Gong, K. Y. Zhang, and S. J. Chua, *J. Vac. Sci. Technol. A* **26**, 1462 (2008).
- <sup>26</sup>J. H. He and C. H. Ho, *Appl. Phys. Lett.* **91**, 233105 (2007).
- <sup>27</sup>X. Li, B. Zhang, H. Zhu, X. Dong, X. Xia, Y. Cui, Y. Ma, and G. Du, *J. Phys. D* **41**, 035101 (2008).
- <sup>28</sup>J. C. Zhang, Y. H. Zhu, T. Egawa, S. Sumiya, M. Miyoshi, and M. Tanaka, *Appl. Phys. Lett.* **92**, 191917 (2008).